International Journal Of
Industrial Electronics Control and Optimization
Print ISSN: 3517-2645
Online ISSN: 3568-2645
Homepage: https://ieco.usb.ac.ir/

On the Advance of Flyback CCM Control Strategies: a Comprehensive Review

Saleh Mohammadi[1] | Hamidreza Izadfar[2] | Naser Eskandarian[2]

[1]Department of Electrical and Computer Engineering, Esfarayen university of technology, Esfarayen, North Khorasan, Iran
[2]Department of Electrical and Computer Engineering, Semnan university, Semnan, Iran
Corresponding author's email: s.mohammadi@esfarayen.ac.ir

Article Info

Article type:
Review Article
Article history:
Received: 20-October-2024
Received in revised form: 10-December-2024
Accepted: 17-December-2024
Published online: 23-Sep-2025
Keywords:
Flyback micro-inverter,
photovoltaic system,
right-half plane,
stability.

ABSTRACT

This research aims to provide a comprehensive review of various CCM control strategies for flyback inverters. The study is carried out based on published data in reports, papers, and other available online documents. The introduced control strategies make use of different approaches to dominate the constraints on determining the feedback control system gains caused by the zero put on right-half-plane (RHP) and dynamics of the LC filter. Thus, the tracking of the considered output current is accurately implemented and the introduced control systems carry out the attenuation of disturbances. Moreover, zero steady-state error and the stability requirements are fulfilled by properly regulating the control signal. The best control structure should be enough fast to employ the fewest number of delays in its structure resulting the burden in the computational system being considerably decreased.

NOMENCLATURE

A_e	Core cross-sectional area	K_I	Integral gain.
A_L	No gap Inductance factor.	L_m	Magnetizing inductance.
B_{sat}	Saturation flux density.	n (N_s/N_p)	Turn ratio of the flyback transformer.
d_{max}	The peak value of the converter duty cycle for DCM state.	N (f_s/f_g)	Control system delays number.
f_g	Frequency of utility voltage.	N_s	Semiconductors total number.
f_s	Switching and sampling frequency.	P_{avg}	The average value of output power
i_g	Current of grid.	R_{pv}	The dynamic resistance of PV
$I_{avgpri,s}$	The average current value associated with the primary side of the transformer in a switching cycle.	T_s	Period of switching
$I_{avgpri,g}$	The average transformer primary current in half of the utility cycle.	v_g	Voltage of grid
i_{pri}	The transformer's primary side current.	V_{rms}	Grid voltage RMS value
I_{rms}	Grid current RMS value.	V_m	The maximum value of utility voltage
I_{pv}	Photovoltaic (PV) module output current	V_{pv}	The PV panel voltage.
k_r	Repetitive controller gain.	ω	The utility voltage angular frequency.

I. Introduction

By enhancing the importance of energy derived from natural sources, photovoltaic (PV) devices have been broadly used in different scopes. The utility-tied photovoltaic systems can be grouped into three main category: the centralized, string, and ac module systems [1]-[6]. Between these systems, the low-power inverter that is stated ac module system or micro-inverter is placed on every photovoltaic system, providing the exclusively tracking the maximum power point (MPP). Consequently, the losses of power owing to inconformity of photovoltaic module and regional shading can be decreased [7]–[11]. In addition, the characteristics

like simpler preservation and high value of the micro-inverter reliability are another advantages of them [12]-[17]. Therefore, the above aspects result the ac-module a suitable method for renewable power generating systems for future times.

While at the nominal power the flyback converter works in CCM in a PV micro-inverter system, entering the DCM at momentary output powers with low values or when decreasing the solar irradiation is an unavoidable phenomenon. Thus, a hybrid operation mode can be considered for the flyback micro-inverter working in the whole utility cycle. The system with low gain is an intrinsic specification of DCM operated flyback converter. As a result, a high gain for the feedback control system should be applied for proper reference signal tracking and complete attenuation of the disturbances. However, the limitation put on the control system gain as a result of zero placed on the right-half-plane (RHP) in CCM while applying the usual PI controller is unavoidable. As a consequence, it results in power quality being unacceptable and the total harmonic distortion being high (THD) due to inaccurate DCM control system performance [18], [19]. This is the main factor for the hybrid mode confined usage of the flyback converter contrary to its outstanding specifications in micro-inverter applications.

Solving the above matter, the static reference frame proportional resonant (PR) controller [20– 22] and the digital repetitive controller [23–25] are reported in the literature. However, the simple approach, little error in steady-state, and little burden in the computational system are some benefits of the PR controller. The decline with the exponential state as a reaction of step change is an example of the constraints of the above controller. In addition, the sensitivity to the variable frequency changes of repetitive signals and the phase shift instability appearing in signals that are measured are other PR controller disadvantages [20–22]. Dealing with periodic signals, the repetitive control method is an efficient scheme. Bode plot infinite amplitudes of this control system at harmonics of the main frequency can result in controller instability. Contrary to different solutions that have been suggested to solve this matter, these schemes suffer from other constraints, such as unacceptable performance responding to disturbances with a non-intermittent nature, slow dynamic response, and vast requirements for memory space [23–25].

The harmonic control array (HCA) method that has been introduced lately, is an appropriate scheme to control systems with intermittent temper such as disturbance and/or reference signals [26-28]. Compensating periodic control signal is easily generated by applying this control scheme, tracking or rejecting considered harmonic components. Moreover, the system gain at the utility frequency and its multiples can be augmented by applying the HCA method. In the mentioned approach, the harmonic contents of the reference and control signals are calculated by using the integral of the Fourier series [26-28]. So, to implement this scheme several delays considering switching frequency should be employed. These delays sometimes cause the system's dynamic response to be unstable and very slow.

In this study, we suggest using the filtered signal instead of applying sluggish or intricate schemes controlling the flyback inverter in the CCM state. The selected structure is very easy to implement and also fast which enhances the control system gain at the utility frequency and corresponding harmonics to boost the tracking operation in both DCM and CCM operation states. Part II concisely investigates the steady-state performance of the two-switch flyback converter. Section III analyzes the control issue and the various control schemes tackling it.

II. The two-switch flyback inverter analysis in steady-state

An Illustration of the flyback two-switch ac-module main circuit is shown in Fig.1 which is composed of the flyback two-switch inverter with turn ratio n (N_s/N_p), decoupling capacitor C_{in}, a current source inverter (CSI) ($S_{ac1} - S_{ac4}$), and an output filter. The switches ($S_{1,2}$) of the flyback inverter operate concurrently with high-frequency to transmit the power of the photovoltaic system to the grid. The sinusoidal waveform is obtained from the rectified one by employing the CSI and injecting it into the grid.

The turned-on switches S_{ac1} and S_{ac4} operate as the utility positive voltage reaches. In the same way, when the negative voltage of utility reaches, S_{ac2} and S_{ac3} are turned on. Fig. 2 illustrates the inverter's main waveforms. While each switching period T_s is enhanced, the current of magnetizing inductance i_{Lm} in DCM becomes zero and the transformer is completely demagnetized. As soon as the next switching cycle starts in CCM operation, and within a switching cycle, the current in magnetizing inductance i_{Lm} is non-zero.

By assuming the lossless operation of the system and by noting the balance of power over the utility period, the output power of the PV module is expressed as [29]

$$P_{pv} = V_{pv} I_{avgpri,g} = V_{pv} I_{pv} = V_{rms} I_{rms} = P_{avg} \qquad (1)$$

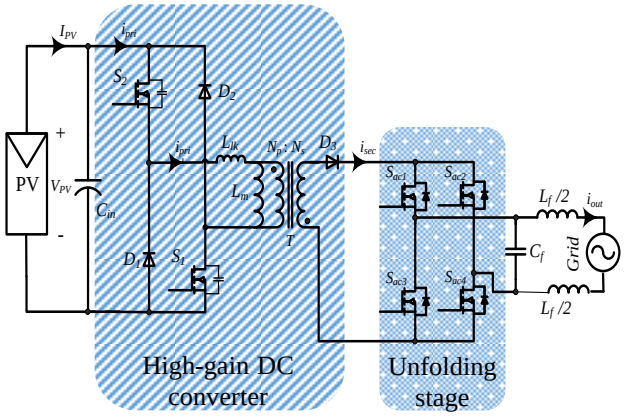

Fig. 1. The flyback two-switch micro-inverter configuration.

In a switching period, by employing the power balance equation, the converter output power can be shown as

$$P_{out}(t) = V_{pv} I_{priavg,s} = v_g(t) i_g(t) = 2 V_{rms} I_{rms} \sin^2(wt) = 2 P_{avg} \sin^2(wt) \qquad (2)$$

In half of the utility period T_h , the average value of the primary current of the transformer is expressed as

$$I_{avgpri,g} = \frac{1}{T_h} \int_0^{T_h} i_{pri}(t)\, dt = \frac{V_{pv} d^2_{\max}}{4 L_m f_s} \qquad (3)$$

Therefore, the calculation of the photovoltaic system output power is obtained as

$$P_{pv} = V_{pv} I_{avgpri,g} = \frac{V^2{}_{pv} d^2{}_{\max}}{4 L_m f_s} \quad (4)$$

Employing the derived equation in (4) we can determine the duty ratio in DCM as follows

$$D_{DCM}(t) = d_{\max} |\sin(\omega t)| = \frac{2}{V_{pv}} \sqrt{P_{pv} L_m f_s} |\sin(\omega t)| \quad (5)$$

The duty ratio and turn ratio *n* are not dependent in the DCM case but the duty ratio is affected by L_m and input power at given specifications in addition to selected frequency f_s. The maximum amount of the primary current in DCM by applying equation (5), is expressed as

$$I_{DCMpri,pk}(t) = \frac{V_{PV} D_{DCM}(t)}{L_m f_s} = 2\sqrt{\frac{P_{avg}}{L_m f_s}} |\sin(\omega t)| \quad (6)$$

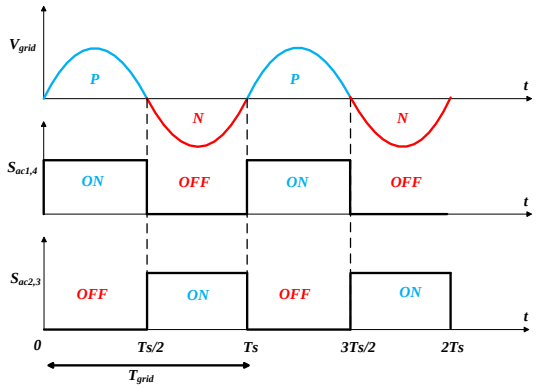

(a)

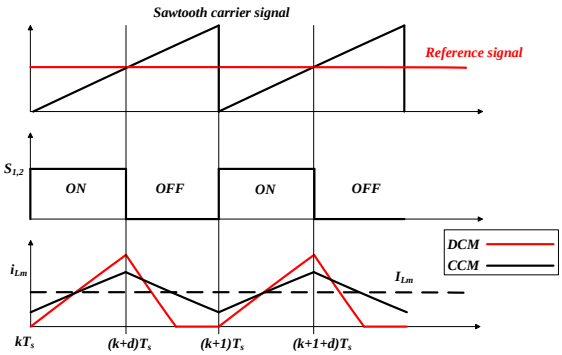

(b)

Fig. 2. The main waveforms of the flyback inverter[37]

Operating the converter in CCM, by using the inductor voltage–seconds law in a switching cycle for L_m, the duty ratio in CCM can be derived as [29]

$$D_{CCM}(t) = \frac{V_g |\sin \omega t|}{n V_{pv} + V_g |\sin \omega t|} \quad (7)$$

However, the converter duty cycle operating in CCM is impressed by the turn ratio n, it doesn't change with input power. The critical magnetizing converter inductance determining the CCM and DCM performance is expressed as

$$L_{mcri} = \frac{V_{pv}}{4 I_{pv} f_s} \frac{1}{(n V_{pv}/V_m + 1)^2} \quad (8)$$

As shown formerly, operated in DCM, the I_{pri} peak magnitude is obtained as (6). Operating in CCM, as illustrated in Fig. 2, to obtain the primary current maximum value $I_{CCMpri,pk}$, adding the two components the mean value of magnetizing current I_{Lm} and the ripple component Δi_{Lm} of that are necessary. Turning on the main switch S_1, the primary current is equal to the magnetizing current.

As a result, by dividing the average primary current and the duty cycle, the magnetizing inductance current average value can be obtained. Thus, the magnetizing inductance current average amount and its ripple component can be expressed as

$$I_{Lm}(t) = \frac{I_{avgpri,s}}{D_{CCM}(t)}$$
$$\Delta i_{Lm} = \frac{V_{pv}}{L_m f_s} D_{CCM}(t) \quad (9)$$

Thus, the maximum amount of primary current $I_{CCMpri,pk}$ is obtained as

$$I_{CCMpri,pk}(t) = \frac{I_{avgpri,s}}{D_{CCM}(t)} + \frac{V_{PV} D_{CCM}(t) T_s}{2 L_m}$$
$$= \frac{P_{out}(t)}{V_{PV}} \times \frac{n V_{PV} + |v_g(t)|}{|v_g(t)|} + \frac{V_{PV}}{2 L_m f_s} \times \frac{|v_g(t)|}{n V_{PV} + |v_g(t)|} \quad (10)$$

At different output powers, the duty cycle variation over half a utility period is illustrated in Fig.3 at specified quantities of f_s, L_m , and *n*. As shown in this scheme, for defined specifications, corresponding to the output power the duty cycle is increased by employing the fixed input voltage. The inverter operates in DCM if the momentary duty cycle at DCM operation mode is lower than the curve of CCM specified with the transformer turn ratio *n* in Fig.3; otherwise, the CCM operation mode is enabled. At a specific power, the CCM duty cycle doesn't intersect with the DCM curve, so the inverter operation is carried out only in the DCM state.

III. The flyback ac-module control structure analysis

A. The flyback ac-module control issue

Time-varying performance and nonlinearity are characteristics of flyback inverter. However, by considering small changes around its operating point it can be considered as a system with a linear time-invariant nature. As a result of changes in the performance, appropriate transfer functions should be derived with regard to each state. Good tracking performance and stability should be considered by the controller in various operating states. Unavoidably working in DCM at low power conditions of the inverter, the transfer function of control to-output current can be determined as

$$G_{id-DCM} = \frac{V_{pv}}{V_{rms}} \sqrt{\frac{P_{avg}}{2 f_s L_m}} \quad (11)$$

This relation specifies a gain with a low value in all frequencies. Having accurate and fast reference tracking and rejection of disturbances performances, the gain of the feedback controller should be enough high in the DCM state. Operating in CCM, the transfer function of the converter can be shown as [30]

$$G_{id-CCM} = \frac{M s^2 + N s + K}{s^2 (R_{pv} C_{in} L_m) + s L_m + D^2{}_{CCM} R_{pv}} \quad (12)$$

where

$$M = -\frac{I_{Lm}}{n} R_{pv} C_{in} L_m$$
$$N = -\frac{I_{Lm}}{n} L_m + R_{pv} C_{in} \frac{(1-D_{CCM})}{n} (V_{pv} + \frac{V_m}{n}) \quad (13)$$
$$K = -D^2_{CCM} R_{pv} \frac{I_{Lm}}{n}$$
$$+ \frac{(1-D_{CCM})}{n} (V_{pv} + \frac{V_m}{n} - D_{CCM} I_{Lm} R_{pv})$$

Observing the relation of (12), $G_{id\text{-}CCM}$ has a zero put on RHP that places limitations on the feedback controller gains satisfying the system stability. Depending on the operating point of the system the RHP zero obtains various quantities. Transferring the maximum power, the minimum value of RHP zero occurs at the maximum value of grid voltage. All the operating points should be covered by the converter's controller, lowering the feedback control system. Moreover, the poles of the operating system are calculated as

$$pole\ (G_{id-CCM}) = -\frac{1}{2} \frac{1}{R_{pv} C_{in}} \pm$$
$$j \frac{1}{2} \frac{\sqrt{L^2_m - 4R^2_{Pv} D^2_{CCM} C_{in} L_m}}{R_{pv} C_{in} L_m} \quad (14)$$

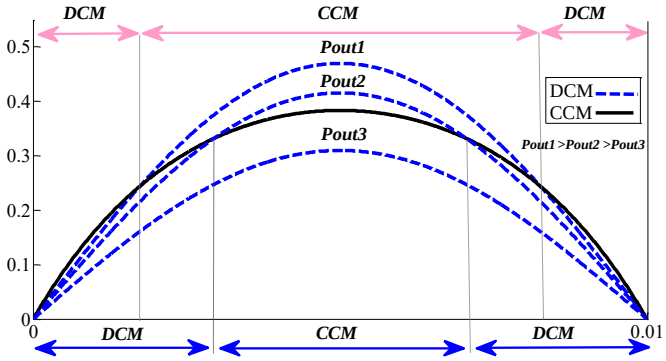

Fig. 3. Variations of duty cycle during half a grid period for CCM and DCM

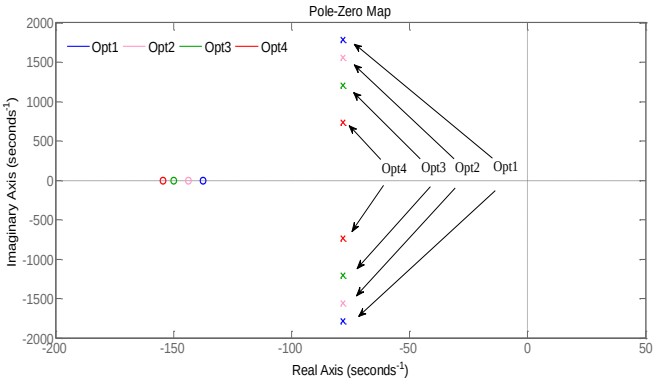

Fig. 4. Placement of Pole-zero for various operating points

TABLE 1 CHARACTERISTICS OF POLE-ZERO FOR FOUR VARIOUS PERFORMANCE STATES

Op. point	D (%)	Pout (W)	I_{Lm} (A)	V_m(V)	Zeroes	Poles
Opt_1	35.01	300	17.13	269.33	$Z_1 = 4.86 \times 10^5$ $Z_2 = -138$	-78.1+/-j1780
Opt_2	30.55	200	13.09	219.9	$Z_1 = 6.36 \times 10^5$ $Z_2 = -144$	-78.1+/-j1560
Opt_3	23.72	100	8.43	155	$Z_1 = 9.88 \times 10^5$ $Z_2 = -150$	-78.1+/-j1210
Opt_4	14.55	30	4.12	85.17	$Z_1 = 2.02 \times 10^6$ $Z_2 = -154$	-78.1+/-j739

According to the calculated relation of (12), the pole-zero scheme is demonstrated in Fig.4. The elaborate analysis of these operating points is also mentioned in Table I. As it is shown, decreasing the output power with instantaneous nature, moving the poles toward the real axis and moving away the zeroes from the origin. From the pole/zero distribution of the system, a non-minimal phase specification due to zero put on RHP is also observable. In addition, the oscillatory of the system is observable by increasing the instantaneous output power.

Compensated system Bode plots utilizing the usual PI controller with two various proportional gains are illustrated in Fig. 5. Table II lists the parameters employed in this study. Satisfying the constraint considering the minimum RHP zero of the inverter, the proportional gain of the controller should be sufficiently low.

In this regard, the gain of the system in the main frequency and its multiples in DCM is lesser than in CCM. This causes the flyback converter incapable of implementing reference tracking and rejecting the disturbances set by the photovoltaic system and utility in DCM. The proportional gain of the controller can be increased to solve this problem. However, the gain of the control system in all frequencies is increased which can make the system unstable as a result of system gain constraint regarding RHP zero. Thus, to design the flyback controller system, choosing the proper gains of the PI controller is a big problem. Various control approaches have been introduced in the literature to solve these control issues which are explained in the following part.

TABLE 2 PARAMETERS OF THE EMPLOYED FLYBACK AC-MODULE

Parameter	value	Unit
Turn ratio of transformers (Np/Ns)	1/10	
Utility voltage and frequency	220/50	V/Hz
Power of output	200	W
Sampling and switching frequency	100	kHz
Input voltage (V_{pv})	50	V
Magnetizing inductance L_m	15	µH
Leakage inductance L_{lk}	0.3	µH
Capacitor C_{in}	6.4	mF
Inductor L_f	3	mH
Capacitor C_f	0.66	µF
Core type		EE42
Rectifier diode	*D3*	IDP12E120
Clamping diodes	*D1, D2*	22GQ100
Main switches	S_1, S_2	IPB107N20N3G
Unfolding bridge switches	S_{ac1}-S_{ac4}	IRFP450B

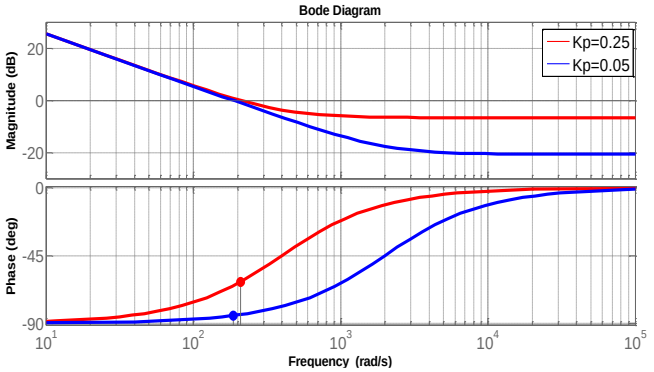

(a)

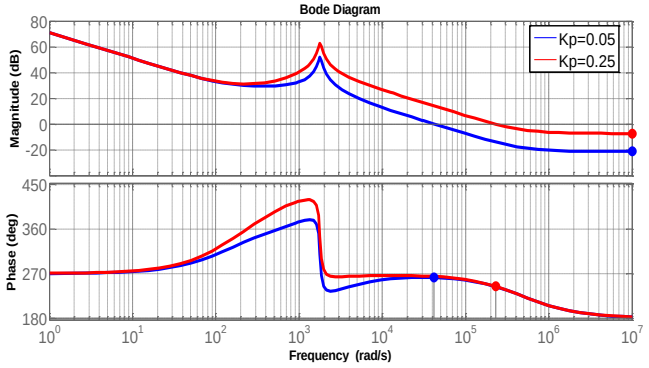

(b)

Fig. 5. The maked-up system Bode plots when the usual PI controller is employed. (a) DCM state. (b) CCM state

B. The Usual Control Systems of Flyback Micro-inverter

Improving the stability of the inverter, the usual control system of the flyback ac-module with the repetitive controller is illustrated in Fig. 6[19]. This control structure preserves the gain of the system high at only the low-frequency region, enhancing the output current tracking performance, while preventing the disturbances of grid voltage at the main and low-order harmonic frequencies. In addition, to compensate for the system phase lag in the repetitive control structure, the phase lead compensator is also employed. The above controller is obtained as

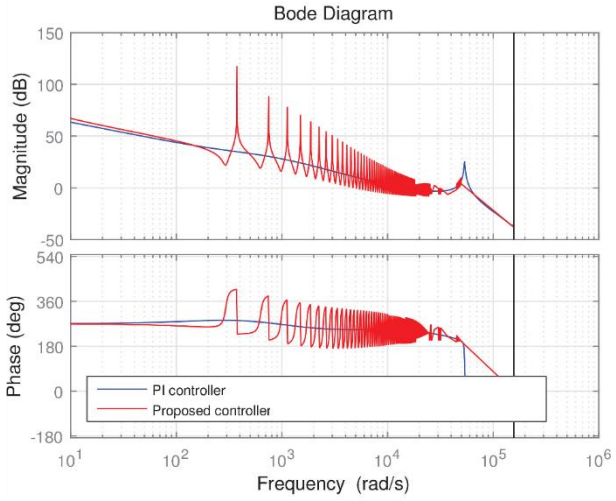

(a)

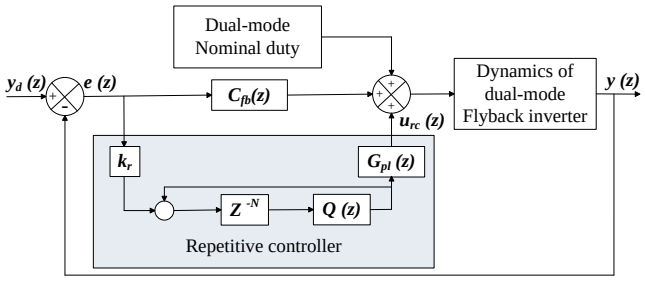

(b)

Fig. 6. Repetitive control structure (a) Bode plot (b) Control block diagram [19]

$$G_{rc}(z) = k_r \frac{z^{-N}Q(z)}{1 - z^{-N}Q(z)} G_{pl}(z) \tag{15}$$

$Q(z)$ is the low-pass filter, and $G_{pl}(z)$ is the system phase lead compensator. As Fig. 6 (b) illustrates and expressed in (15), the control system's large delays cause the dynamics of the system to be slowed down and may lead to system instability. Moreover, the Bode plot infinite amplitudes of this controller at harmonics of the main frequency can cause instability of the control system.

Indirectly controlling the output current [Fig.7] which controls the input current of the converter is applied in [29], [34] and [35]. Concerning fast and proper reference tracking performances, it is not as efficient as direct control schemes. Subharmonics phenomena and bifurcation are observable in the charge control approach under certain operating conditions [36]. Mitigating the oscillation and unsuitable operation of the usual control structure, a fourth-order model of the converter has been derived in [30]. This model of the converter including the output filter is calculated as

$$G_{id-CCM} = \frac{ps^3 + As^2 + Bs + C}{s^4 + Es^3 + Fs^2 + Hs + M} \tag{16}$$

Where A, B, C, E, F, H, M,and p are calculated in [30].The bode plot comparison of second and fourth-order models is shown in Fig. 8. As it is shown, the fourth-order model shows a resonant peak and sudden phase drop at a specified frequency. Thus, designing the appropriate controller including the output CL filter can be a big challenge. Employing the lag term with a conventional PI controller is proposed in this paper. The damping term is derived as

$$C_{lag} = \frac{1}{2.5 \times 10^{-5} s + 1} \tag{17}$$

The proposed controller is shown in Fig.9 and the bode plot of the compensated system is illustrated in Fig. 10. Although the suggested design structure of the decoupled two-stage controller is systematic way, it is a process with intricate and Time-consuming nature to determine the lag term appropriately and precisely.

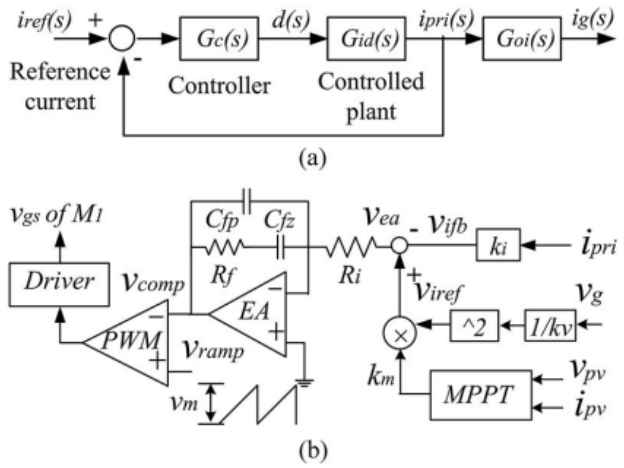

Fig.7.Controlling the flyback converter with an indirect manner[29] (a) Control block diagram(b) Detailed control system

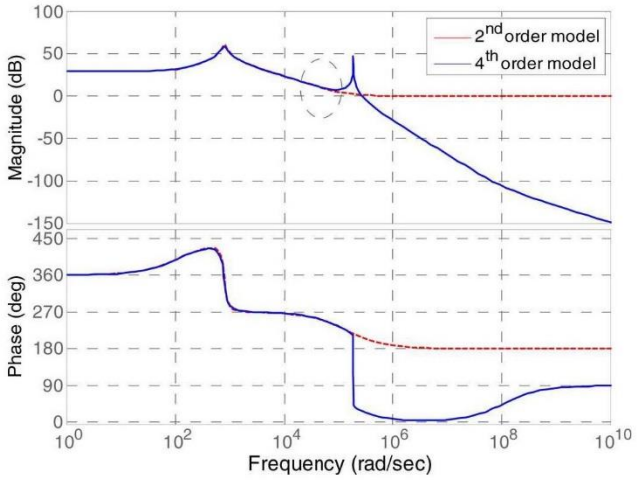

Fig.8. The bode plot comparison of second and fourth-order models [30]

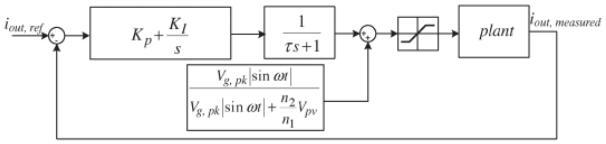

Fig.9. The proposed control system in [30]

Enhancing the stability of the usual flyback ac-module control system with the PR controller has been illustrated in Fig. 11. By applying the PR controller with HCs (harmonic compensators), high gain at the main frequency of the utility and its harmonics is reached. In addition, the bandwidth in DCM is enhanced. Thus, tracking of the reference and rejecting the disturbances as well as the suitable stability in both DCM/CCM states are fulfilled [18], [38]. The above controller with resonant gain k_{rf}, proportional gain k_p ,and cut-off frequency ω_c is expressed as

$$C_{PR}(s) = k_p + \frac{2k_{rf}\omega_c s}{s^2 + 2\omega_c s + \omega^2} \tag{18}$$

Putting the HC to the mentioned system, the errors of the considered harmonic frequencies can be alleviated, and its transfer

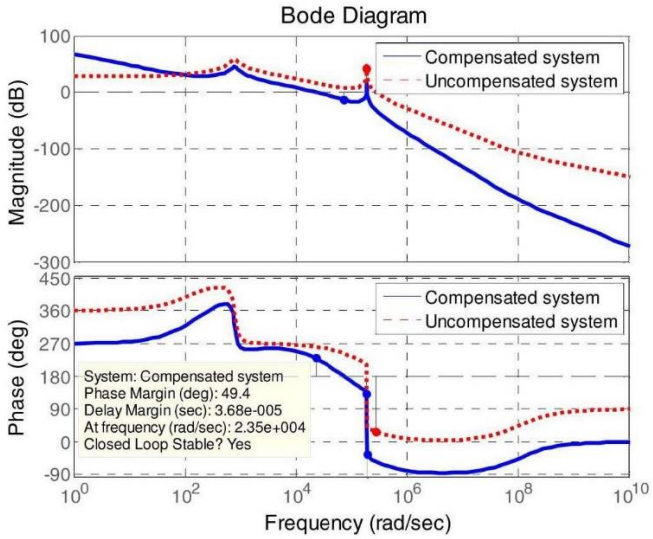

Fig.10. The bode plot of the compensated system [30]

function with the resonant gain for each harmonic k_{rfl} is expressed as

$$C_{HC}(s) = \sum_{l=3,5,7,\ldots} \frac{2k_{rfl}\omega_c s}{s^2 + 2\omega_c s + (l\omega)^2} \tag{19}$$

As expressed in Fig. 11 (b) and stated in (18) and (19), slowing down the dynamic of the system and the possibility of unacceptable effects on the operation of the system are the consequences of adding multiple harmonic frequencies to the controller. In addition, the availability of the infinite amplitudes in the controller's Bode diagram at considered harmonic frequencies can result in instability of the control system.

Fig. 12 shows another flyback micro-inverter control system that can be employed [27]. Employing a gain with great value at the frequency of the grid and its harmonics without a high proportional gain is the property of the current control system with a harmonic control array (HCA) structure. Thus, in this scheme, the reference signal is tracked easily with zero error in steady-state accompanied by the satisfaction of the appropriate CCM stability. Three stages of this control approach are determined as:

1- The dispersing unit to diffuse harmonics

$$< x >_h [n] = \frac{1}{N}\sum_{k=n-N+1}^{n} x[k]e^{-jh\omega kT_s} = \frac{1}{N}\sum_{k=n-N+1}^{n} x[k]e^{-j2\pi hk/N} \tag{20}$$

2- The assembling unit to collect harmonics

$$f[n] = < f >_0 [n] + 2\,\mathrm{Re}\left\{\sum_{h=1}^{H} < f >_h [n] e^{j2\pi hn/N}\right\} \tag{21}$$

3- The controller section to control the whole process

$$< f > [n] = K_p < e > [n] + K_I E[n] \tag{22}$$

As it is shown in Fig. 12 and (20)-(22), several large delays are employed in the HCA control system that slow down the dynamics of the converter, and the stability of the system can be affected.

Moreover, the requirement of large memory space is another challenge of this approach.

C. Selection of the best control approach

As stated, the usual control systems present unacceptable performances concerning the aforementioned converter control problem. To have a proper and stable performance in hybrid

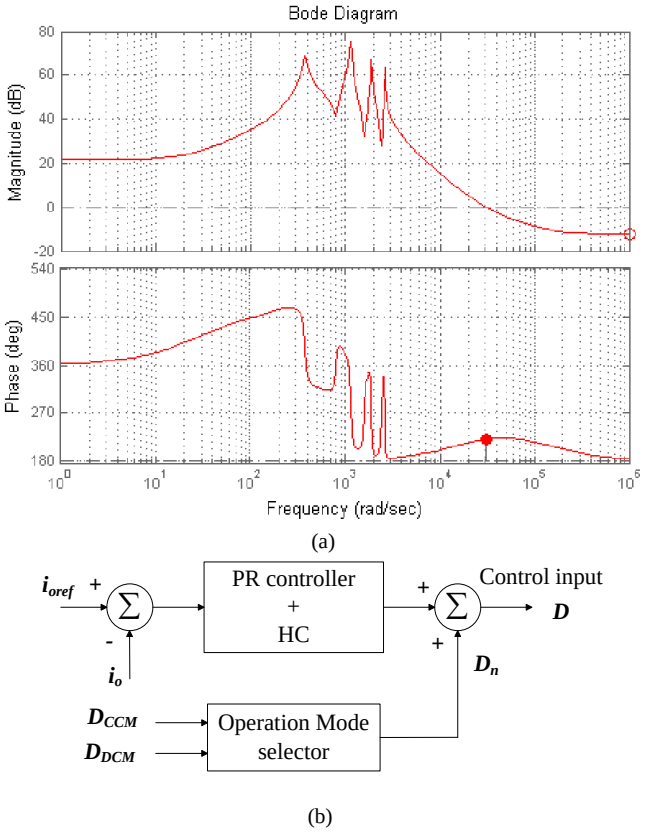

Fig. 11. Control structure of PR (a) Bode plot (b) Control block diagram [18]

CCM/DCM state, the main solution is selecting the controller gains proportional to frequency. As a result, we suggest a very simple but highly effective control structure that has been introduced in [37]. A PI control system accompanied by a low pass filter that permits only the main frequency and its low order harmonics to go across the system. The suggested control structure has a significantly fast response that is performed easily in the low-frequency section with a large proportional gain. As a result, proper implementation in both CCM and DCM states is guaranteed. The employed filter with low pass characteristics in the suggested system is determined as

$$G_f(z) = \frac{1}{\tau((1-z^{-1})f_s)+1} \tag{23}$$

where $\tau = 1/2\pi f_c$ with cut-off frequency $f_c(Hz)$. The suggested control scheme is illustrated in Fig. 13 whose simplicity and fast response are superior to the other control approaches such as repetitive controller, PR as well as HCA. The compensated system Bode plot with the presented control system is illustrated in Fig. 14. It is shown that the high gain at low order harmonics with the suggested control system is provided modifying the tracking speed and disturbance rejection performances accompanied with stability in both CCM and DCM operation states.

Various CCM control approaches employed in flyback ac-module are compared in Table III. As it is shown, the best tracking speed is presented with the aforementioned control structure and also it applies a little burden in the computational system approximately between all of the other control approaches. Moreover, the primary switches' voltage stresses are limited to the DC input voltage employing the two-switch scheme of the converter leading to using the switches with low voltage rating with low conduction losses.

IV. Conclusion

This paper presented a detailed survey of the various control structures introduced to solve the problems that come from the control to output current transfer function zero put on the right-half-plane (RHP) in the flyback micro-inverters. The working principle of each structure, features, restrictions, and recent status were investigated. As a general result, a PI controller with a low pass filter has a better performance against different types of control systems. In the mentioned control scheme, a high system gain at the main frequency and its multiples is provided with the usual PI controller accompanied by a low-pass filter. The usual control problem existing in flyback ac-modules operated at CCM is solved with this control system. It imposes an accurate and suitable DCM tracking operation and acceptable CCM stability. Also, the selected control approach presents little burden in the computational system and has a suitable dynamic response that does not exist in the usual control systems. Furthermore, the disturbances are better rejected and tracking of reference in conjunction with the other control systems is faster implemented.

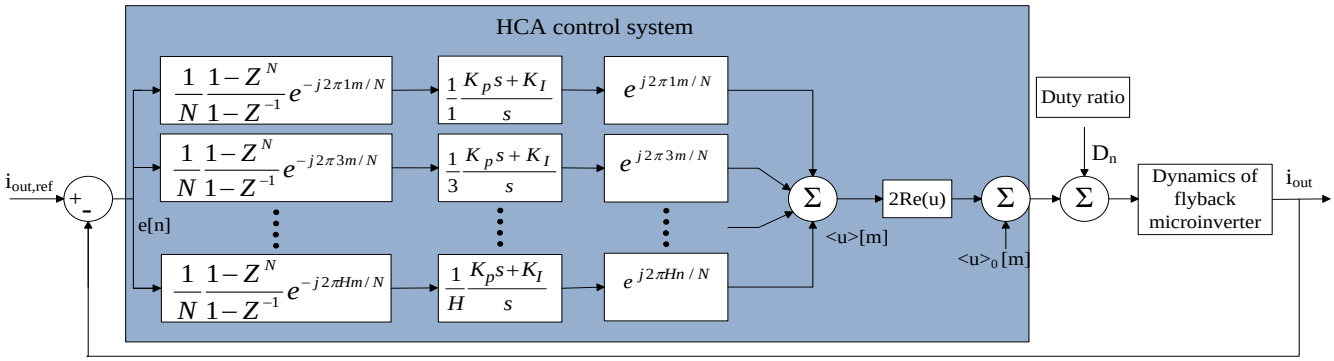

Fig. 12. The control scheme for HCA-based system [27]

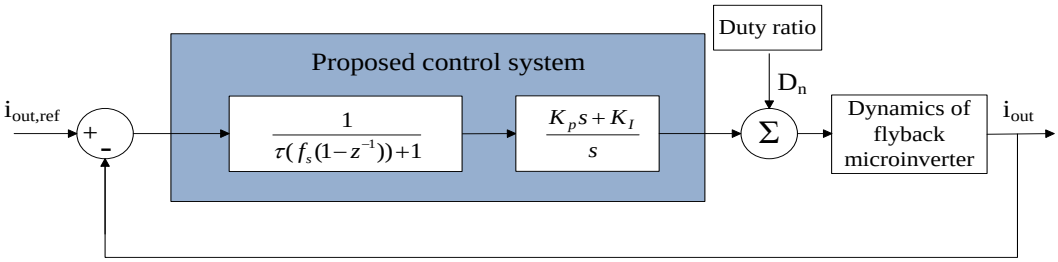

Fig. 13. The suggested control approach in [37]

TABLE 3
THE COMPARISON OF VARIOUS CCM CONTROL APPROACHES EMPLOYED IN FLYBACK AC-MODULE

Reference	Control parameter	controller	Tracking speed	Memory space requirement	Voltage stress of main switches	Power factor	MPPT efficiency (%)	MPPT Voltage range (V)	THD (%)	Efficiency (%)	**Approximate power [W]**
[18]	Output current	PR+HC	medium	large	$V_{PV}+V_m/n$	-	-	40-80 & V_{mpp}=60	2.4	96.1	**200**
[19]	Output current	repetitive	low	large	V_{PV}	-	98.5	V_{mpp}=60	2.4	96.3	**200**
[29]	Input current	type II	medium	small	$V_{PV}+V_m/n$	0.99	98	V_{mpp}=27	<5	87.4	**200**
[30]	Output current	type II	high	small	$V_{PV}+V_m/n$	-	-	25-55 & V_{mpp}=55	4	95.7	**200**
[33]	Output current	repetitive	low	large	V_{PV}	-	-	V_{mpp}=48	2.9	96	**200**
[34]	Input current	type II	medium	small	$V_{PV}+V_m/n$	-	99.5	V_{mpp}=35.6	5	90	**200**
[35]	Input current	type II	medium	small	$V_{PV}+V_m/n$	0.99	98	V_{mpp}=27	-	86.8	**200**
[36]	Input current	Charge control	medium	small	$V_{PV}+V_m/n$	0.99	98	20-27 & V_{mpp}=27	1.56	-	**200**
[37]	Output current	PI	high	small	V_{PV}	>0.98	-	V_{mpp}=50	-	96.1	**200**
[38]	Output current	PR+HC	medium	large	$V_{PV}+V_m/n$	-	-	-	2.34	-	**200**
[39]	Output current	PR+HC	medium	large	$V_{PV}+V_m/n$	-	-	V_{mpp}=38.9	2.27	94.5	**200**
[40]	Output current	PR+HC	medium	large	$V_{PV}+V_m/n$	-	-	V_{mpp}=28.7	2.1	-	**200**

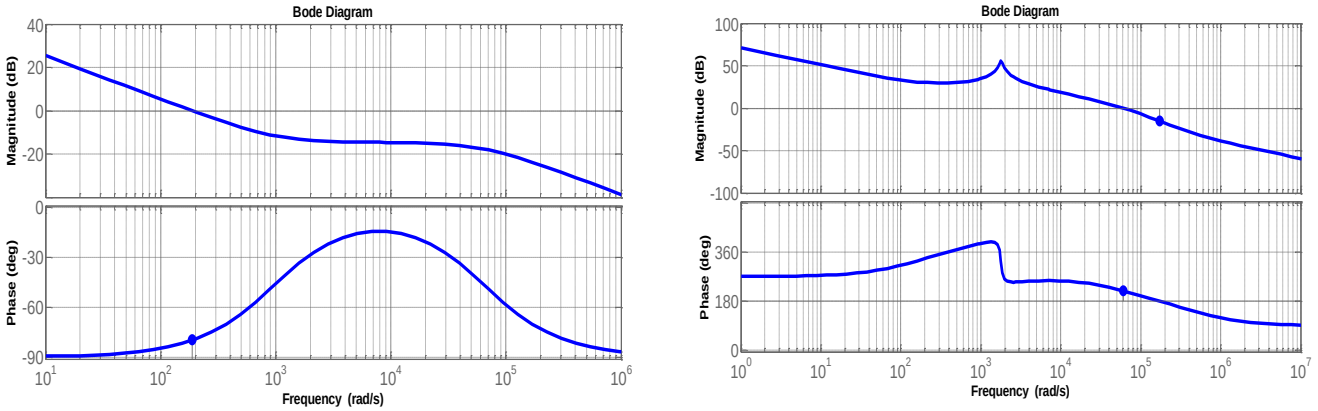

(a) (b)

Fig. 14. Open-loop Bode plots of the maked-up system by the selected appropriate controller. (a) In DCM. (b) In CCM

REFERENCES

[1] A. Mousaei, M. Gheisarnejad, M.H. Khooban, Challenges and opportunities of FACTS devices interacting with electric vehicles in distribution networks: A technological review, Journal of Energy Storage, Volume 73, Part A, 2023,108860,ISSN2352-152X,https://doi.org/10.1016/j.est.2023.108860

[2] Kim YH, Jang JW, Shin SC, Won CY. Weighted-efficiency enhancement control for a photovoltaic AC module interleaved flyback inverter using a synchronous rectifier. IEEE transactions on power electronics. 2014 Feb 13;29(12):6481-93.

[3] Rezaei MA, Lee KJ, Huang AQ. A high-efficiency flyback micro-inverter with a new adaptive snubber for photovoltaic applications. IEEE transactions on Power Electronics. 2015 Mar 5;31(1):318-27.

[4] Sukesh N, Pahlevaninezhad M, Jain PK. Analysis and implementation of a single-stage flyback PV microinverter with soft switching. IEEE transactions on industrial electronics. 2013 May 17;61(4):1819-33.

[5] Gao M, Chen M, Zhang C, Qian Z. Analysis and implementation of an improved flyback inverter for photovoltaic AC module applications. IEEE transactions on Power Electronics. 2013 Aug 27;29(7):3428-44.

[6] Christidis GC, Nanakos AC, Tatakis EC. Hybrid discontinuous/boundary conduction mode of flyback microinverter for AC–PV modules. IEEE Transactions on Power Electronics. 2015 Aug 19;31(6):4195-205.

[7] Kyritsis AC, Tatakis EC, Papanikolaou NP. Optimum design of the current-source flyback inverter for decentralized grid-connected photovoltaic systems. IEEE transactions on energy conversion. 2008 Feb 15;23(1):281-93.

[8] Mohammadi S, Izadfar HR, Eskandarian N. A new adaptive clamp for improving weighted efficiency in grid-tied photovoltaic interleaved two-switch flyback micro-inverter.

International Transactions on Electrical Energy Systems. 2019 Aug;29(8):e12033.

[9] Zhang F, Xie Y, Hu Y, Chen G, Wang X. A hybrid boost–flyback/flyback microinverter for photovoltaic applications. IEEE Transactions on Industrial Electronics. 2019 Feb 11;67(1):308-18.

[10] Sarikhani A, Allahverdinejad B, Hamzeh M, Afjei E. A continuous input and output current quadratic buck-boost converter with positive output voltage for photovoltaic applications. Solar Energy. 2019 Aug 1;188:19-27.

[11] Rahimi R, Farhangi S, Farhangi B, Moradi GR, Afshari E, Blaabjerg F. H8 inverter to reduce leakage current in transformerless three-phase grid-connected photovoltaic systems. IEEE Journal of Emerging and Selected Topics in Power Electronics. 2017 Aug 23;6(2):910-8.

[12] Mohammadi S, Zarchi HA. An interleaved high-power two-switch flyback inverter with a fast and robust maximum power point tracker. In2016 7th Power Electronics and Drive Systems Technologies Conference (PEDSTC) 2016 Feb 16 (pp. 320-325). IEEE.

[13] Mohammadi S, Zarchi HA, Amiri M. Interleaved two-switch flyback microinverter for grid-tied photovoltaic applications. InThe 6th Power Electronics, Drive Systems & Technologies Conference (PEDSTC2015) 2015 Feb 3 (pp. 59-64). IEEE.

[14] Wang F, Feng X, Zhang L, Du Y, Su J. Impedance-based analysis of grid harmonic interactions between aggregated flyback micro-inverters and the grid. IET Power Electronics. 2018 Mar;11(3):453-9.

[15] Keshani M, Adib E, Farzanehfard H. Micro-inverter based on single-ended primary-inductance converter topology with an active clamp power decoupling. IET power electronics. 2018 Jan;11(1):73-81.

[16] Mohammadi S, Izadfar HR, Eskandarian N. Performance optimisation of the grid-connected flyback inverter under improved hybrid conduction mode. IET Renewable Power Generation. 2020 Oct;14(13):2437-46.

[17] Dong D, Agamy MS, Harfman-Todorovic M, Liu X, Garces L, Zhou R, Cioffi P. A PV residential microinverter with grid-support function: Design, implementation, and field testing. IEEE Transactions on Industry Applications. 2017 Sep 14;54(1):469-81.2

[18] Lee SH, Cha WJ, Kwon JM, Kwon BH. Control strategy of flyback microinverter with hybrid mode for PV AC modules. IEEE transactions on industrial electronics. 2015 Sep 23;63(2):995-1002.

[19] Kim S, Lee SH, Lee JS, Kim M. Dual-mode flyback inverters in grid-connected photovoltaic systems. IET Renewable Power Generation. 2016 Oct;10(9):1402-12.

[20] Kim S, Lee SH, Lee JS, Kim M. Dual-mode flyback inverters in grid-connected photovoltaic systems. IET Renewable Power Generation. 2016 Oct;10(9):1402-12.

[21] Mousaei, A.; Naderi, Y. Optimal Predictive Torque Distribution Control System to Enhance Stability and Energy Efficiency in Electric Vehicles. Sustainability 2023, 15, 15155. https://doi.org/10.3390/su152015155.

[22] Karbasforooshan MS, Monfared M. Multi-resonant indirect digital current control technique for single-phase shunt active power filters. Electric Power Components and Systems. 2019 Aug 9;47(13):1196-202.

[23] Mattavelli P, Marafao FP. Repetitive-based control for selective harmonic compensation in active power filters. IEEE Transactions on Industrial Electronics. 2004 Oct 4;51(5):1018-24.

[24] Geng H, Zheng Z, Zou T, Chu B, Chandra A. Fast repetitive control with harmonic correction loops for shunt active power filter applied in weak grid. IEEE Transactions on Industry applications. 2019 Jan 25;55(3):3198-206.

[25] Pandove G, Singh M. Robust repetitive control design for a three-phase four wire shunt active power filter. IEEE Transactions on Industrial Informatics. 2018 Oct 9;15(5):2810-8.

[26] Dogruel M, Çelik HH. Harmonic control arrays method with a real time application to periodic position control. IEEE transactions on control systems technology. 2010 May 6;19(3):521-30.

[27] Karbasforooshan MS, Monfared M, Dogruel M. Application of the harmonic control arrays technique to single-phase stand-alone inverters. IET Power Electronics. 2016 Jun;9(7):1445-53.

[28] Karbasforooshan MS, Monfared M, Dogruel M. Indirect control of single-phase active power filters using harmonic control arrays. In2017 Conference on Electrical Power Distribution Networks Conference (EPDC) 2017 Apr 19 (pp. 143-148). IEEE.

[29] Li Y, Oruganti R. A low cost flyback CCM inverter for AC module application. IEEE transactions on Power Electronics. 2011 Aug 18;27(3):1295-303.

[30] Edwin FF, Xiao W, Khadkikar V. Dynamic modeling and control of interleaved flyback module-integrated converter for PV power applications. IEEE transactions on industrial electronics. 2013 Apr 16;61(3):1377-88.

[31] Sharifi S, Monfared M, Nikbahar A. Highly efficient single-phase direct AC-to-AC converter with reduced semiconductor count. IEEE Transactions on Industrial Electronics. 2020 Feb 5;68(2):1130-8.

[32] Choi HS. Transformer Design Consideration for off-line Flyback Converters using Fairchild Power Switch. Fairchild Semiconductor App. Note AN4140. 2004:1-0.

[33] Jeong YS, Lee SH, Jeong SG, Kwon JM, Kwon BH. High-efficiency bidirectional grid-tied converter using single power conversion with high-quality grid current. IEEE Transactions on Industrial Electronics. 2017 May 11; 64(11):8504-13.

[34] Thang TV, Thao NM, Jang JH, Park JH. Analysis and design of grid-connected photovoltaic systems with multiple-integrated converters and a pseudo-dc-link inverter. IEEE Transactions on industrial electronics. 2013 Sep 9; 61(7):3377-86.

[35] Li Y, Oruganti R. A low cost high efficiency inverter for photovoltaic AC module application. In2010 35th IEEE Photovoltaic Specialists Conference 2010 Jun 20 (pp. 002853-002858). IEEE.

[36] Li Y, Oruganti R. A flyback-CCM inverter scheme for photovoltaic AC module application. Australian Journal of Electrical and Electronics Engineering. 2009 Jan 1; 6(3):301-9.

[37] Mohammadi S, Izadfar HR, Eskandarian N. A simple and highly efficient flyback inverter control strategy for AC module application. IET Power Electronics. 2022 Oct 31

[38] M. Dong and X. Tian, "Dual-Mode interleaved flyback micro-inverter," 2017 Chinese Automation Congress (CAC), Jinan, China, 2017, pp. 7719-7724, doi: 10.1109/CAC.2017.8244175.

[39] Yang Jian and Ye Bingqing, "Accurate modeling and sliding mode control method to improve the current sharing performance for PV grid-connected interleaved flyback mirco-inverter," 2016 IEEE International Conference on Power and Renewable Energy (ICPRE), Shanghai, 2016, pp. 558-564, doi: 10.1109/ICPRE.2016.7871138.

[40] D. L. Caiza, S. Kouro, F. Flores-Bahamonde and R. Hernandez, "Unfolding PV Microinverter Current Control: Rectified Sinusoidal vs Sinusoidal Reference Waveform," 2018 IEEE Energy Conversion Congress and Exposition (ECCE), Portland, OR, USA, 2018, pp. 7094-7100, doi: 10.1109/ECCE.2018.8558024.

Saleh Mohammadi recieved his Ph.D. degree in power Engineering from the University of Semnan, Iran in 2020 wth an honor. In 2024, he joined the Department of Electrical and Computer Engineering at Esfarayen University of Technology, Esfarayen, Iran. His research interests include, power electronics and active filters.

Naser Eskandarian is currently an Assistant Professor in the Electrical and Computer Engineering Department of Semnan University. His research interests include computer control, robotics, power electronics, and electric vehicles. He has managed several industrial projects, some of which have won international awards.

Hamid Reza Izadfar is currently an Associate Professor in the Electrical and Computer Engineering Department of Semnan University. His main research interests are the design and analysis of electric machines and drives.